Journal of Electronic Materials (2024) 53:5118–5129
https://doi.org/10.1007/s11664-024-11160-3

28TH INTERNATIONAL CONFERENCE ON NUCLEAR TRACKS AND RADIATION MEASUREMENTS

Impact of Dispersion of V-TiO_2/$MoSe_2$/MoO_3 Composite on the Dielectric Properties of 8CB Liquid Crystal

Nidhi[1] · Jai Prakash[1] · Shikha Chauhan[1] · Magan Himanshu[2] · Kamlesh Yadav[2,3]

Received: 25 January 2024 / Accepted: 2 May 2024 / Published online: 27 May 2024

Abstract
Owing to sensitivity to external perturbations such as temperature, electric field, and magnetic field, the dielectric and electro-optical properties of liquid crystals (LCs) can be easily tuned. In recent years, the dispersion of nanomaterials into LCs has proven to be an important tool for the fabrication of various devices with improved characteristics. In the present study, we have synthesized a nanocomposite of vanadium-doped titanium oxide (VTO) with the integration of molybdenum diselenide ($MoSe_2$) and molybdenum trioxide (MoO_3), designated as VTO-MSE (V-TiO_2/$MoSe_2$/MoO_3), through a hydrothermal procedure and measured the dielectric features of 4′-octyl-4-biphenylcarbonitrile (also known as 8CB) LC material doped with the VTO-MSE nanocomposite at different concentrations (0.1 wt.%, 0.25 wt.%, 0.5 wt.% and 1 wt.%) in smectic A (SmA) and nematic (N) phases of 8CB at 28 °C and 36 °C, respectively. The uniform dispersion of VTO-MSE in 8CB was confirmed using polarizing optical microscopy, and the dielectric measurements were performed using frequency-dependent dielectric spectroscopy in the frequency range of 20 Hz–2 MHz. The dielectric parameters (ε' and ε'') decreased on the dispersion of the nanocomposite in 8CB LC in the low-frequency region due to the reduction of mobile ions. The peak of the dielectric loss factor (tan δ) also shifted towards the low-frequency side because of the decrease in the mobile ion density. The threshold voltage was found to decrease for the VTO-MSE-mixed 8CB samples and dielectric anisotropy was also obtained, which shows an increase in its value for the nanocomposite dispersed systems. These results can be beneficial for the manufacture of display devices.

Keywords Nematic liquid crystal · smectic liquid crystal · nanocomposite · dielectric properties

Introduction

Liquid crystals (LCs) act as soft smart materials due to their controllable responsive and adjustable nature which makes them favourable for display and non-display applications.[1] The LC is the state of matter intervening between crystalline solids and isotropic liquids with anisotropic electrical, optical, and magnetic properties. Depending on their molecular symmetry, they are categorized as nematic, smectic, and cholesteric phases, where the nematic phase possesses a long-range orientational order while the smectic has some positional order along the orientational order.[2–6] LC-based display devices deal with certain issues such as image sticking, slow responses, high threshold voltages, and reduced voltage holding ratio due to the presence of mobile ions that degrade their performance. When an electric field is applied to these systems, the ions move towards the electrode surface, are adsorbed there, and thus create their own field which reduces the effect of the applied electric field.[7] Several efforts have been made to solve these issues, and two approaches have been considered by researchers. The first is the synthesis of a new LC with desirable properties and the other is the use of certain guest materials to disperse in the host LC to tune their properties.[8,9] Nanomaterials

✉ Jai Prakash
jpsphysics@gmail.com

✉ Shikha Chauhan
niharikavatsa21@gmail.com

[1] Department of Physics, Aligarh Muslim University, Aligarh, Uttar Pradesh 202002, India

[2] Department of Physics, School of Basic Sciences, Central University of Punjab, Bathinda, Punjab 151401, India

[3] Department of Physics, University of Allahabad, Prayagraj, Uttar Pradesh 211002, India

such as nanoparticles, nanotubes, and nanorods have been dispersed in LC to tailor their electro-optical and electrical properties.[10–13] These methods for tuning LC properties are much faster and more feasible. Nanomaterials trap or adsorb mobile ions on their surface when dispersed in LC, which in turn reduces ion concentration and improves the performance of display devices.[14] Recently, nanocomposites have proved to be potential guest entities for dispersion in LC by altering their physical properties. Several studies have been conducted on TiO_2 nanoparticle-doped LC, as they exhibit both ion trapping and releasing behaviour in different LC matrixes.[7,14–16] When transition metals such as vanadium (V) are doped in TiO_2 nanoparticles, they alter the bandgap and change the polymorph form of TiO_2, which can be useful for certain electrical devices.[17,18] Molybdenum diselenide ($MoSe_2$), which belongs to the family of transition metal dichalcogenides, shows magnificent electrical conductivity, high carrier mobility, and indirect-to-direct bandgap transition due to its layered structure and two-dimensional nature, making it suitable for applications in electronics, optoelectronics, and devices related to energy.[19–21] In addition, molybdenum trioxide (MoO_3) exhibits high electrical conductivity, exceptional stability, and versatile electrochemical properties that can be used for various applications in diverse fields such as in gas sensors, catalysis, energy storage, and optical applications.[22,23] The combination of vanadium-doped titanium dioxide (VTO) with $MoSe_2$ and MoO_3 forms the V-TiO_2/$MoSe_2$/MoO_3 (VTO-MSE) ternary composite with the unique amalgamation of physical, chemical, optical, electrical, and dielectric properties, offering unprecedented potential in LC systems. The physical attributes of the VTO-MSE nanocomposite are poised to redefine material functionalities, seamlessly combining the high surface area and structural stability of VTO with the layered structures of $MoSe_2$ and MoO_3, enhancing the mechanical strength and flexibility.[24,25] The anticipated catalytic properties arising from the interaction between these components hold promise for influencing the chemical stability and responsiveness of the LC matrix. This aspect is particularly appealing for applications that demand meticulous control of chemical interactions. Optical considerations are paramount in advanced material design, and the VTO-MSE composite, with its distinctive combination of materials, exhibits a diverse optical response. Vanadium doping introduces specific absorbance characteristics, complemented by the wavelength-dependent optical properties of the layered structures in $MoSe_2$ and MoO_3.[26] Integrating the composite into LCs has the potential to influence the electrical behaviour of the matrix, thereby expanding its utility in diverse electronic applications. Moreover, considering the dielectric properties, the layered structures within the VTO-MSE composite significantly contribute to its dielectric characteristics, influencing the response of the material to electric fields.[27] This feature is significant in the context of potential integration into LC materials, where dielectric properties play a vital role in controlling the phase transitions and molecular orientations. In essence, the dispersion of nanocomposites in LC introduces a new dimension to the synergy between materials and applications, with the potential to induce transformative changes in the behaviour of the LC matrix. This multifaceted introduction sets the stage for a comprehensive exploration of the impact of composites on LC technologies, ushering in a new era of functional and tailored material applications.

In this article, we present the synthesis of VTO-MSE nanocomposites through a hydrothermal process and their dispersion in an LC material, namely 8CB. We observe the impact of the nanocomposites on 8CB using polarized optical microscopy and frequency-dependent dielectric spectroscopy. Significant changes are observed in the dielectric parameters of the VTO-MSE-mixed 8CB samples compared with the pristine counterpart. Temperature-dependent dielectric measurements are performed in planar and homeotropic orientations, and the threshold voltage is determined for the pure and composite systems. We expect that these results will be advantageous for the fabrication of LC-based display devices.

Experimental Details

Synthesis of V-TiO_2/$MoSe_2$/MoO_3 (VTO-MSE) Nanocomposite

The chemical reagents used for the synthesis were obtained from Sigma-Aldrich and were used without additional purification. The materials included titanium(IV) isopropoxide (97%), ammonium metavanadate extra-pure AR (99%), selenium powder (Se), sodium molybdate dihydrate (SMD), and hydrazine hydrate (HH, 50–60%). Distilled water (DW) was meticulously prepared in the laboratory using the Arium® Pro DI-T ultrapure water system. Analytical-grade absolute ethanol (>99%), obtained from Changshu Hongsheng Fine Chemicals Co., Ltd., was employed both for cleaning purposes and as a solvent in the experimental procedures. A precipitation method was used to prepare V-TiO_2. The precursors for titanium and vanadium were taken in a molar ratio of 9:1. First, ammonium metavanadate was mixed with 20 mL of DW followed by sonication for 15 min for proper suspension of the particles, and maintained under stirring at 40°C. Titanium isopropoxide was then added dropwise to the mixture. After successful precipitation, it was centrifuged followed by oven drying, and was then calcined at 600°C for 2 h. The synthesis of the V-TiO_2 (9)/$MoSe_2$/MoO_3(1) (9:1 M) composite involved a hydrothermal procedure. First, solution (i) was prepared by combining 10 mL of hydrazine

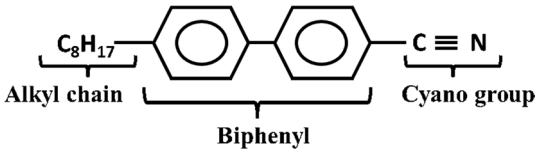

Fig. 1 The chemical structure of 4′-octyl-4-biphenylcarbonitrile (8CB).

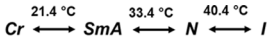

Where Cr, SmA, N and I represents crystalline, smectic A, nematic and isotropic phases respectively.

Fig. 2 The phase transition of 8CB.

hydrate (HH) and selenium (Se) powder, and this mixture was magnetically stirred at room temperature for an entire day. Solution (ii) was prepared by mixing the as-prepared V-TiO_2 (200 mg) in 20 mL ethanol. Simultaneously, solution (iii) was prepared by stirring a blend of 20 mL distilled water (DW) and 10 mL ethanol with sodium molybdate dihydrate (SMD). Achieving suitable suspensions required subjecting solutions (i) and (iii) to sonication for 15 min. Subsequently, solution (iii) was gradually introduced into solution (i), and the resulting mixture was agitated for 15 min, after which solution (ii) was also added to this mixture and maintained under stirring for 1 h. The amalgamated solution was then placed in a 100-mL autoclave for 24 h at 200°C in a furnace. After cooling, the solution was washed multiple times using distilled water and ethanol. The resulting material was dried in an oven for 8 h at 70°C.

Liquid Crystal Material Used

We used 4′-octyl-4-biphenylcarbonitrile, often called 8CB, as LC material for our experiment, which was procured from Sigma-Aldrich. Its chemical formula is $C_{21}H_{25}N$. The 8CB material comprises a biphenyl group with an alkyl chain and a cyano group attached to the sides as shown in Fig. 1. It has two LC phases, i.e., smectic A (SmA) and nematic (N). The phase sequence of 8CB is shown in Fig. 2.[28]

Preparation of VTO-MSE-LC Composite

First, the VTO-MSE nanocomposite was dispersed in toluene and ultrasonicated for 1 h in order to obtain a uniform dispersion. Measured amounts of this dispersion were then added to the 8CB material to obtain 0.1 wt.%, 0.25 wt.%, 0.5 wt.%, and 1 wt.% concentrations of VTO-MSE nanocomposite in 8CB. This LC nanocomposite mixture was then sonicated for 10 min at 45°C (above the isotropic temperature of 8CB) to acquire the stable dispersion of nanocomposite and LC material. The mixture was kept in an oven at 115°C, which is above the boiling point of toluene, leaving only VTO-MSE and 8CB material.

Sample Cell Details

The nanocomposite mixed LC material was filled in commercially available sample cells (Instec, Inc., Boulder, CO, USA) for dielectric and optical measurements. The thickness of the sample cells was 5 µm with an active area of 100 mm^2. These cells have glass substrates with indium tin oxide (ITO) films coated on them, and the contact of both electrodes was made on the lower sheet. Then the polyamide layer was rubbed onto the ITO films to obtain a homogeneous alignment of the molecules. The sample cells were filled with pure and nanocomposite mixed LC materials through capillary action.

Instruments

Dielectric measurements were carried out using an LCR meter (E4980A, Keysight, USA) in a frequency range of 20 Hz–2 MHz for the pure and composite systems which were connected to a temperature controller (mk2000, C100W, Instec, Inc., USA). The dielectric parameters were studied under alternating current (AC) voltage of 500 mV in the LC sample cells. The optical textures were obtained using a polarizing optical microscope (BX53M, Olympus, Japan) fitted with a charge-coupled device (CCD) camera.

Results and Discussion

Structural and Optical Properties of VTO-MSE Nanocomposite

The structural composition and phase identity of the synthesized composite VTO-MSE were investigated via x-ray diffraction (XRD). The XRD pattern, graphically represented in Fig. 3, reveals distinct sharp peaks corresponding to each component, confirming the crystalline nature of the composite. The well-defined peaks associated with vanadium-doped titanium dioxide (VTO), molybdenum diselenide ($MoSe_2$), and molybdenum trioxide (MoO_3) confirm the integrity and crystallinity of the individual constituents within the composite. The pattern analysis of VTO revealed distinct diffraction peaks of anatase and rutile phases, indicating the presence of two crystalline phases within the VTO. Anatase peaks (green diamonds) appear at 26.13°, 37.73°, 38.68°, 49.05°, 54.82°, 55.96°, 63.62°, 69.87°, 70.89°, 75.93°, 83.67°, and 85.22°, corresponding to the (101), (103), (004), (200), (105), (211), (204), (116), (220), (215), (312), and (224) planes, respectively (JCPDS 21-1272). Rutile peaks

(black diamonds) appear at 28.31°, 36.81°, 39.37°, 42.07°, 44.86°, 55.17°, 57.53°, and 64.94°, corresponding to the (110), (101), (200), (111), (210), (211), (220), and (200) planes, respectively (JCPDS 21-1276).

Diffraction peaks present at 11.71°, 30.09°, and 51.90° represent the hexagonal crystal structure of $MoSe_2$ (JCPDS 29-0914), and correspond to the (002), (110), and (110) planes, respectively, whereas the diffraction peaks at 23.71° and 44.00° correspond to the (110) and (320) planes of α-MoO_3 (JCPDS 21-0569), respectively. $MoSe_2$ and MoO_3 are present at approximately 6% and 3.5%, respectively, in the prepared sample, which is calculated by comparing with the intensity of peaks using the following equation

$$\text{Fraction}\,(\%)\,\text{of}\;\; MoSe_2 \,\text{or}\, MoO_3 = \frac{\sum I_{MoSe_2\,\text{Or}\;MoO_3}}{\sum I_{\text{Composite}}} \times 100 \tag{1}$$

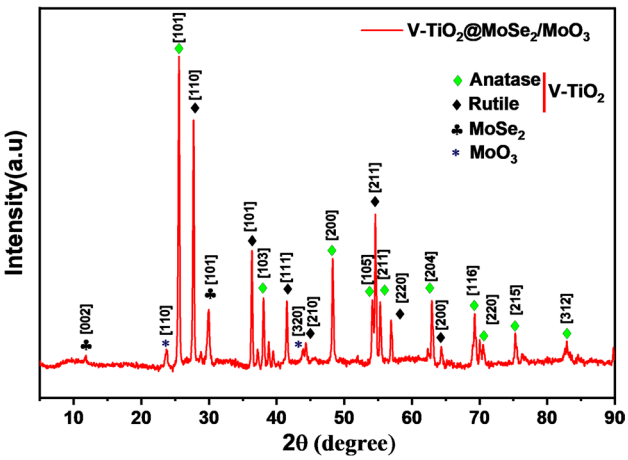

Fig. 3 X-ray diffraction pattern of the as-synthesized nanocomposite (VTO-MSE).

where $I_{MoSe_2 OrMoO_3}$ and $I_{\text{Composite}}$ represent the intensity of peaks of $MoSe_2$ or MoO_3 and the composite, respectively.

Figure 4a depicts absorbance versus wavelength plots for the composite V-TiO_2/$MoSe_2$/MoO_3 between 200 nm and 900 nm. A gradual increase in absorbance can be observed from 900 nm to 300 nm. The inset shows the Tauc plot for the calculation of the bandgap. The calculated bandgap of the composite (~1.5 eV) is less than the bandgap of V-doped TiO_2 (~2.0 eV).[27,29] Figure 4b shows the Fourier transform infrared (FTIR) spectrum of the composite V-TiO_2/$MoSe_2$/MoO_3. The presence of Mo–Se (740 cm^{-1}) and Mo=O (905 and 944 cm^{-1}) groups confirms the successful synthesis of the $MoSe_2$ and MoO_3 components.[30–32]

Additionally, the distinctive vibration mode of Ti–O (665 cm^{-1}) further confirms its incorporation of VTO into the composite.[33] The high-intensity peak corresponding to Ti–O bonds further confirms the presence of the highest amount of VTO in the composite. The N–H bonds (1400, 2378 cm^{-1}) correspond to the amine groups attached to the surface of the composite.[34,35] The presence of C=O bonds (1630 cm^{-1}) suggests the presence of carbonyl groups. The C–O stretch (2309 cm^{-1}) denotes the presence of ether or carbonyl groups. Unsaturated C=C bonds, C–H stretching peaks (2854, 2924 cm^{-1}), and O–H peak (3423 cm^{-1}) appear in the FTIR spectra. All these functional groups attached to the nanocomposite, introducing intermolecular interactions that modify the properties of the LC.[36]

Figure 5a and b display the field emission scanning electron microscopy (FESEM) image and energy-dispersive x-ray (EDX) spectra of a ternary composite, V-TiO_2/$MoSe_2$/MoO_3, showcasing three distinctive morphologies: agglomerated V-TiO_2 spherical nanoparticles, $MoSe_2$ nanorods, and MoO_3 microrods. The V-TiO_2 nanoparticles have an average size of 85 nm, offering a large surface area and enhanced interfacial interactions. These properties influence the viscosity and flow characteristics of liquid crystal mixtures, while also improving compatibility with liquid crystal

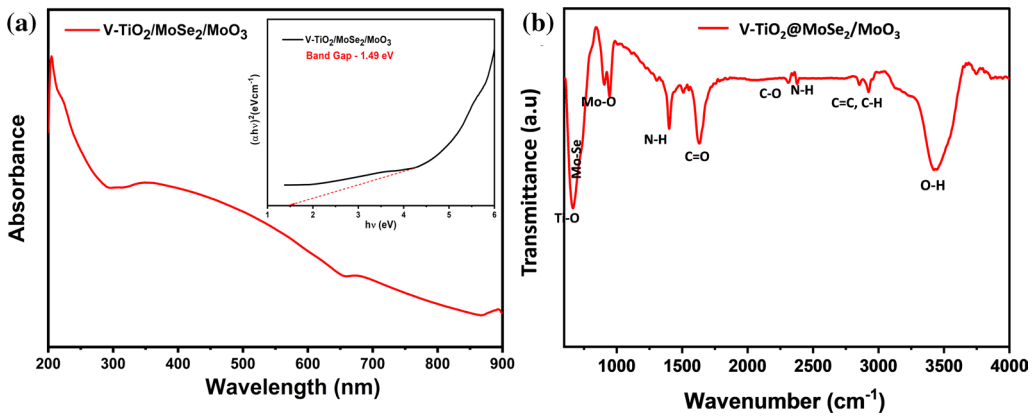

Fig. 4 (a) UV-visible absorbance spectra, inset shows the Tauc plot for the calculation of bandgap, (b) IR transmittance spectra.

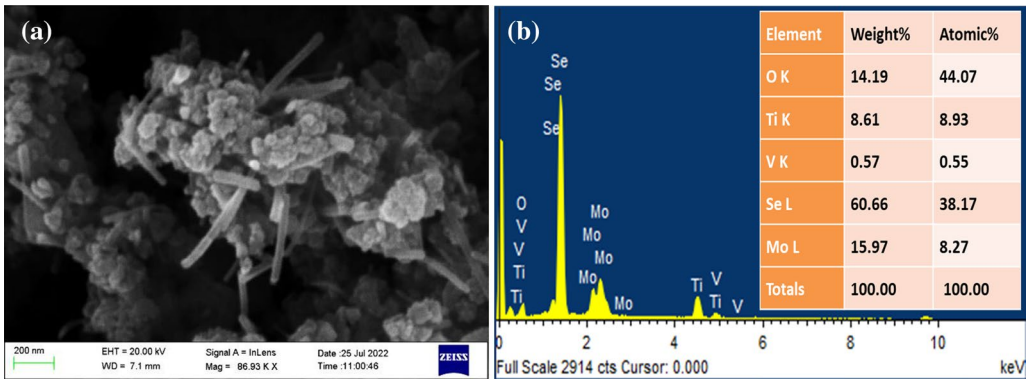

Fig. 5 (a) FESEM images (b) EDX spectra with elemental ratios of as prepared composite.

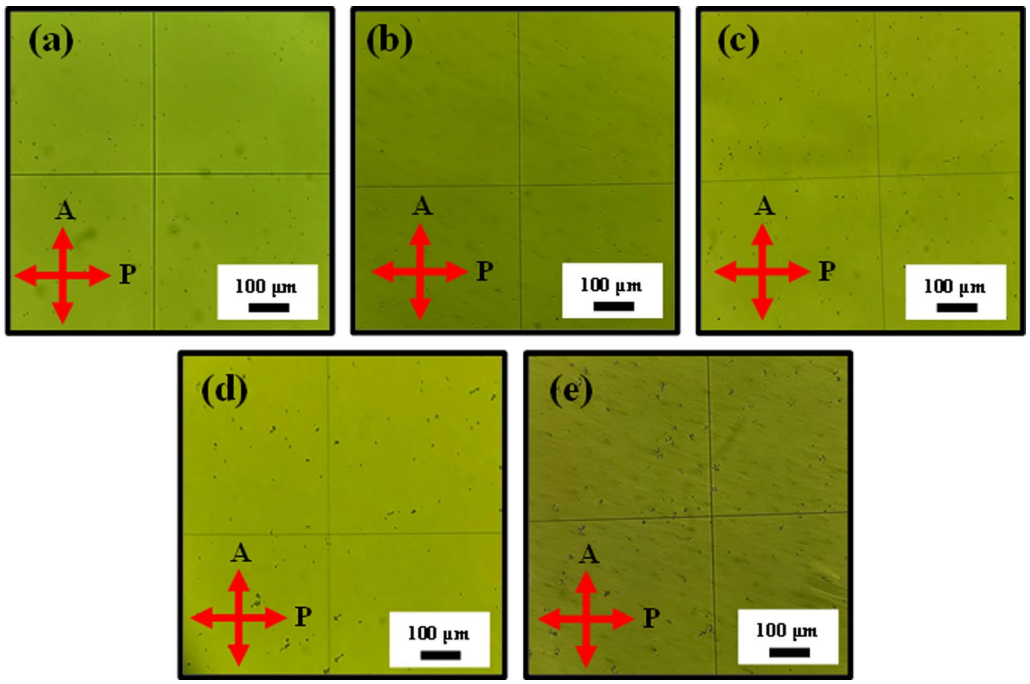

Fig. 6 Polarizing optical micrographs of uniformly aligned LC sample cells with thickness of 5 µm at 0 V bias with (a) 0.0 wt.%, (b) 0.1 wt.%, (c) 0.25 wt.%, (d) 0.5 wt.%, and (e) 1 wt.% of VTO-MSE nanocomposite in 8CB at 28°C (SmA phase). The crossed arrows represent the crossed position of polarizer (P) and analyzer (A). Scale bar: 100 µm.

matrices, thereby promoting homogeneity and stability.[37,38] The elongated and anisotropic shape of $MoSe_2$ nanorods, with an average diameter of 33 nm, enables alignment with liquid crystal molecules, which is crucial for optimal optical performance.[39,40] MoO_3 microrods, which are larger than nanorods, aid in better dispersion within liquid crystal matrices, preventing agglomeration, ensuring uniform distribution, and enhancing stability in the liquid crystal matrix.[41,42] Figure 5b shows the EDX spectra analysis which confirms the successful incorporation of vanadium, titanium, molybdenum, selenium, and oxygen as per the stoichiometry ratio. The absence of extra peaks in the EDX plot confirms the high purity of the as-prepared composite.

Polarizing Optical Microscopy

The optical micrographs were observed by keeping the sample cells under the crossed polarizers for pure 8CB and VTO-MSE nanocomposite-mixed 8CB in both the SmA and N phases at 28°C and 36°C, respectively, as depicted in Figs. 6 and 7. The micrographs had a uniform colour, which suggests that there is a homogeneous and

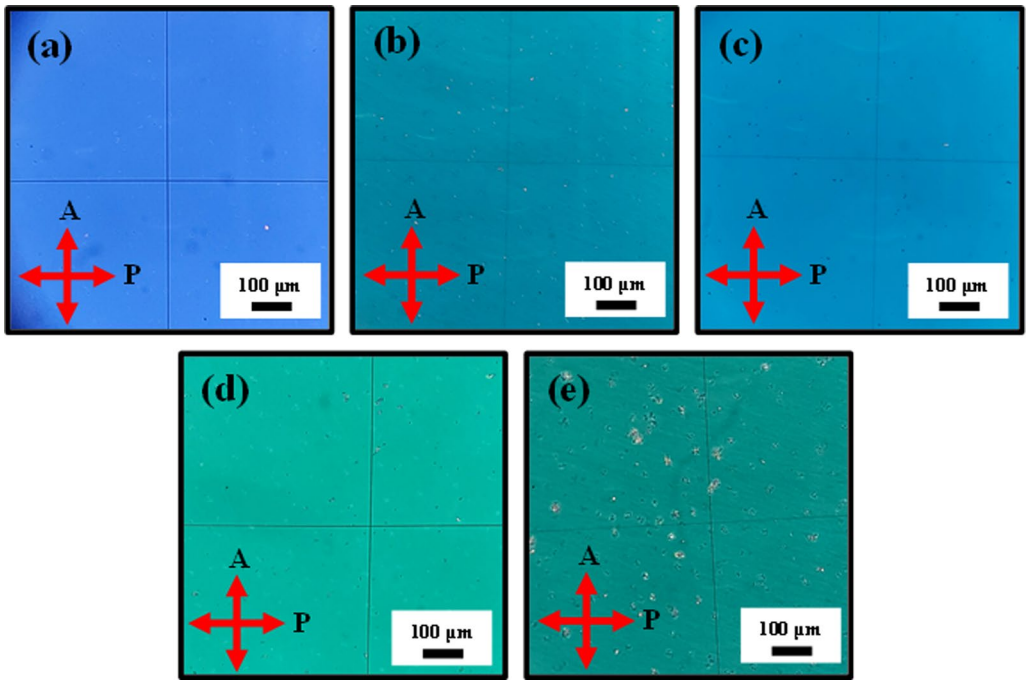

Fig. 7 Polarizing optical micrographs of uniformly aligned LC sample cells with thickness of 5 µm at 0 V bias with (a) 0.0 wt.%, (b) 0.1 wt.%, (c) 0.25 wt.%, (d) 0.5 wt.% and (e) 1 wt.% of VTO-MSE nanocomposite in 8CB at 36°C (N phase). The crossed arrows represent the crossed position of polarizer (P) and analyzer (A). Scale bar: 100 µm.

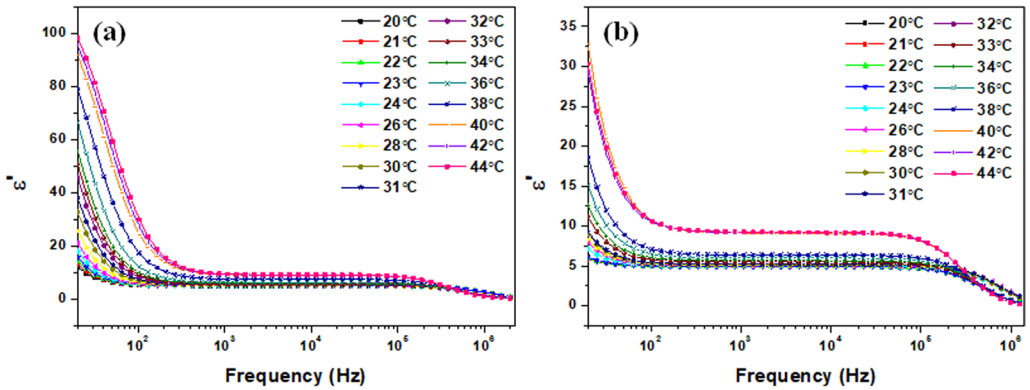

Fig. 8 Variation in dielectric permittivity (ε') with frequency at different temperatures at 0 V biasing for (a) pure 8CB and (b) 0.1 wt.% VTO-MSE-mixed 8CB sample.

agglomeration-free molecular alignment of the composite in the sample cells.

Dielectric parameters

The real (ε′) and imaginary (ε″) parts of dielectric permittivity were calculated using the dielectric spectroscopy and were plotted with respect to frequency at different temperatures varying from 20°C to 44°C for pure 8CB and 0.1 wt.% VTO-MSE-mixed 8CB at 0 V biasing as represented in Figs. 8 and 9. In the low-frequency region, the value of ε′ increases with a decrease in frequency due to the space charge and interfacial polarization caused by the faster movement of ions towards the electrode than the rate of change in polarity of the applied electric field. This increase in ε′ is also attributed to the Maxwell–Wagner polarization in which the dielectric is considered as inhomogeneous medium with conducting grains which are separated by the grain boundaries that are resistive in nature. When the electric field is applied to the dielectric, space charges accumulate near the grain boundaries which are more dominant than the grains, and hence we observe the greater value of ε′ at

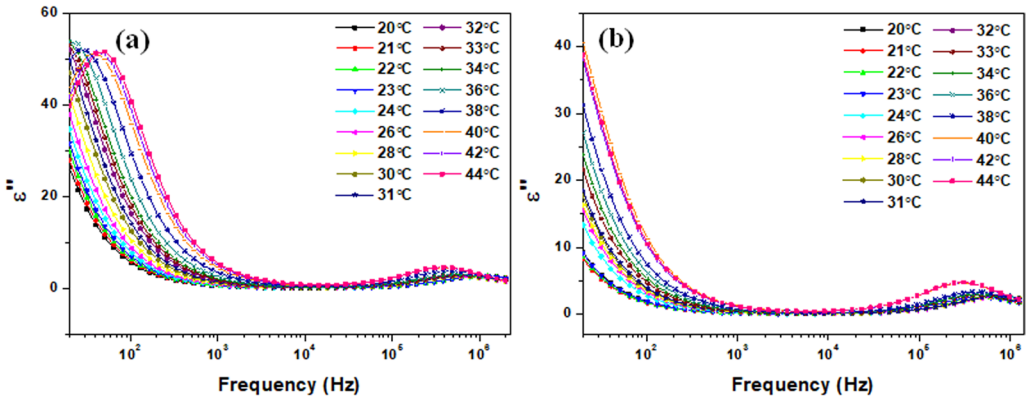

Fig. 9 Variation in dielectric loss (ε'') with frequency at different temperatures at 0 V biasing for (a) pure 8CB and (b) 0.1 wt.% VTO-MSE-mixed 8CB sample.

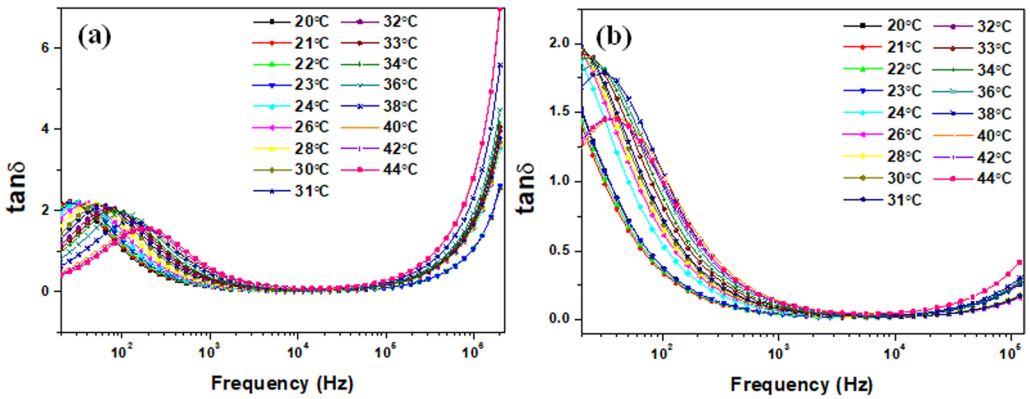

Fig. 10 Variation in dielectric loss factor (tan δ) with frequency at different temperatures at 0 V biasing for (a) pure 8CB and (b) 0.1 wt.% VTO-MSE-mixed 8CB sample.

low frequency.[43] As the frequency increases, ε' decreases and attains a constant value and further decreases at high frequency as the ions no longer follow the electric field. It was observed that the value of ε' increases with temperature due to the disordering of the molecules at increased temperature. Furthermore, the sudden increase in the value of ε' corresponds to the transition of the LC material from the nematic phase to the isotropic phase. In the dielectric loss or ε'' graph, two peaks were observed, one in the low-frequency region which is attributed to the electrode and space charge polarization, and the other in the high-frequency region which arises due to molecular rotation.[44] Moreover, the peak in the lower-frequency region shifts towards the high-frequency side with an increase in temperature due to the increased rotational viscosity in the medium.[45]

The dielectric loss factor or tan δ is defined as tan $\delta = \varepsilon''/\varepsilon'$, which represents the energy dissipation in the dielectric system. Figure 10 illustrates the variation in tan δ with respect to frequency at different temperatures for pure 8CB and 0.1 wt.% VTO-MSE nanocomposite-mixed 8CB material at 0 V biasing. A low-frequency peak is observed in both samples which appears due to the relaxation of ions in the lower-frequency region as they accumulate near the electrode surface.[46] This peak shifts towards the high-frequency side as the temperature increases due to the space charge polarization of mobile ions present in the sample that shift towards the high-frequency region with the increasing temperature.

Figure 11 shows the plot of ε' with frequency for various concentrations of VTO-MSE nanocomposite-mixed 8CB material at 0 V biasing for SmA and nematic phases at 28°C and 36°C, respectively. The value of ε' decreases when the VTO-MSE nanocomposite is dispersed in 8CB as compared with pure 8CB in the lower-frequency region for 0.1 wt.% and attains almost the same value for 0.25 wt.%, 0.5 wt.% and 1 wt.%. The greatest changes are observed for 0.1 wt.%, which is considered to be the optimum concentration. The adsorption of ions on the surface of the nanocomposite leads

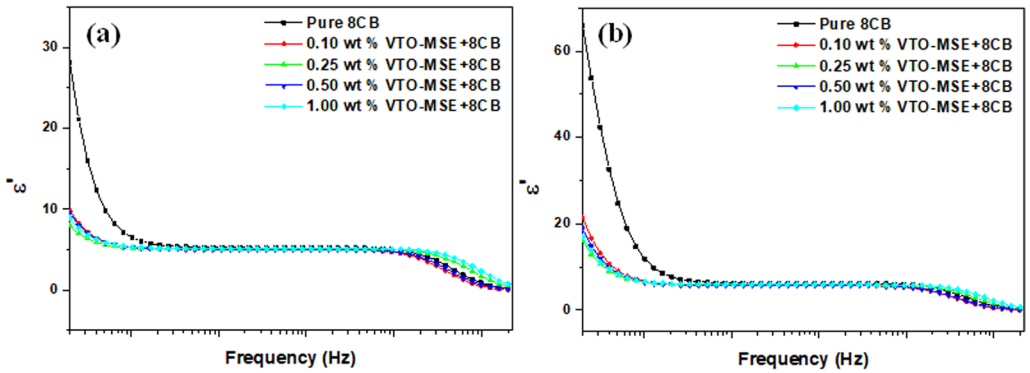

Fig. 11 Variation in dielectric permittivity (ε') with respect to frequency at 0 V bias for (a) smectic and (b) nematic phases for pure and composite samples.

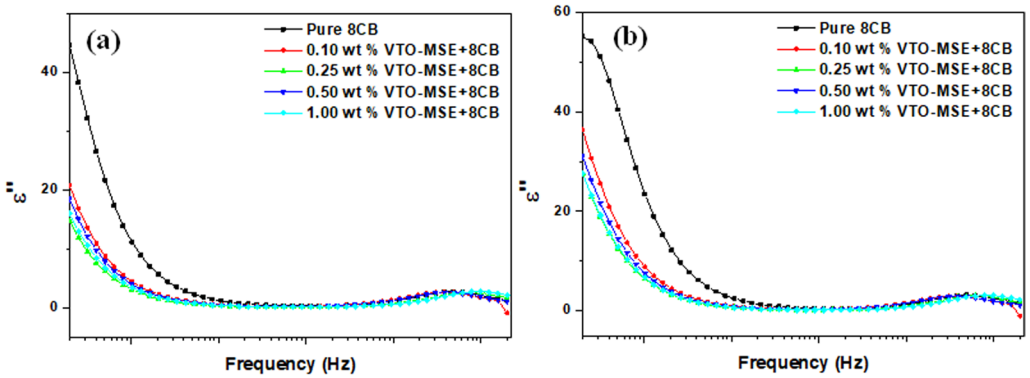

Fig. 12 Variation in dielectric loss (ε'') with respect to frequency at 0 V bias for (a) smectic and (b) nematic phases for pure and composite samples.

to a decrease in the number of ions in the low-frequency region, resulting in a low value of ε′. Accordingly, the value of ε″ decreases for VTO-MSE-dispersed 8CB in the low-frequency regime as shown in Fig. 12 due to the reduction in ionic impurities upon the addition of nanocomposite. The dielectric spectra can be evaluated using the following equations developed by Uemura to describe the motion of mobile ions under the effect of a small alternating field in the low-frequency region

$$\varepsilon' = \frac{2nq^2D^{3/2}}{\varepsilon_0 d\pi^{1/2}k_BT} f^{-3/2} \tag{2}$$

$$\varepsilon'' = \frac{2nq^2D}{\varepsilon_0 k_B \mathrm{T}} f^{-1} \tag{3}$$

where n represents the density of the mobile ions, q is the electrical charge, D is the diffusion coefficient of the ions, d is the thickness of the cell, ε_0 is the dielectric permittivity of free space, k_B is the Boltzmann constant, T is the temperature, and f is the frequency.[47,48] The ε' and ε'' are directly proportional to the ion density as indicated by these equations, and thus their reduced value on the dispersion of the nanocomposite in pure LC depicts the decrease in the density of mobile ions.

The variation in tan δ with respect to frequency for different concentrations of VTO-MSE-dispersed 8CB at 0 V for SmA and N phases at 28°C and 36°C, respectively, is given in Fig. 13. The value of tan δ decreases with frequency in the low-frequency region, which can be explained on the basis of the Koops model. According to this model, the dielectric consists of two layers: one represents the grains, which is the conducting layer, and the other is the grain boundaries, which is the non-conducting layer. The conducting layer is effective at high-frequency regions, and thus we obtain a lower value of tan δ, while the grain boundaries are prevalent at lower frequencies due to high resistivity which contributes to the higher value of tan δ.[49,50] The relaxation peak in the lower-frequency region shifts towards the low-frequency side on the dispersion of VTO-MSE in the 8CB material. This shift can be

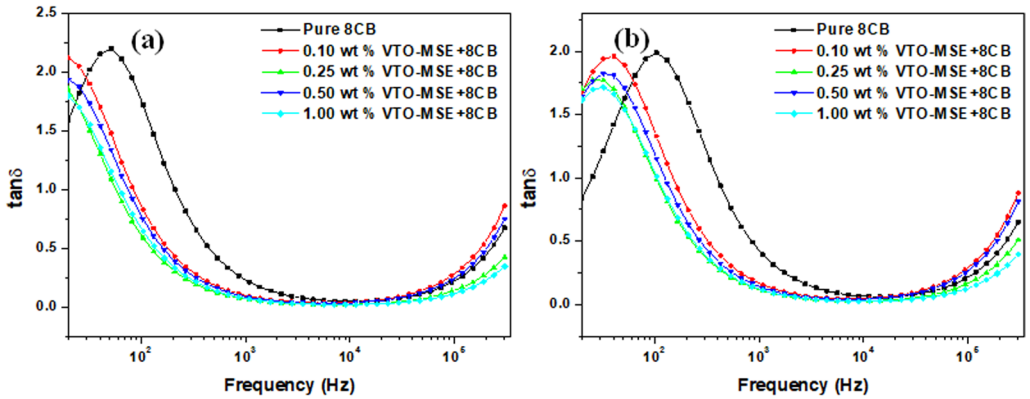

Fig. 13 Variation in dielectric loss factor (tan δ) with respect to the frequency at 0 V bias for (a) smectic and (b) nematic phase for pure and composite samples.

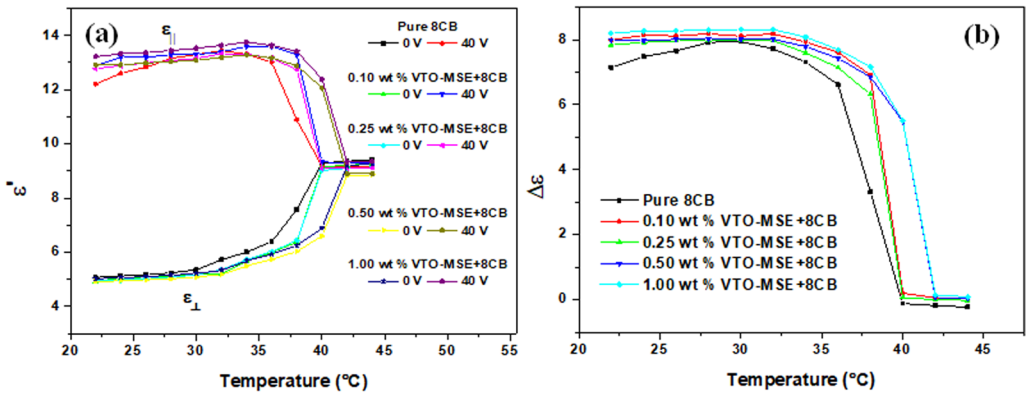

Fig. 14 Temperature-dependent (a) parallel and perpendicular components of ε' and (b) $\Delta\varepsilon$ of 8CB and VTO-MSE in 8CB composite for different concentrations at 1 kHz.

ascribed to the reduced rotational viscosity of the LC due to the trapping of ions by the nanocomposite.

Dielectric Anisotropy

Dielectric anisotropy ($\Delta\varepsilon$) is the difference in dielectric permittivity between the homeotropic and planar orientations. It is defined as

$$\Delta\varepsilon = \varepsilon_{\parallel} - \varepsilon_{\perp} \tag{4}$$

where $\varepsilon_{\parallel}$ is the parallel component of dielectric permittivity when the molecules orient in the parallel direction to the electric field (homeotropic orientation) and $\varepsilon_{\perp}$ is the perpendicular component of dielectric permittivity when the molecules align in the perpendicular direction to the electric field (planar orientation).[51,52] These measurements were not taken in the low-frequency region where mobile charge polarization processes occur at a frequency of 1 kHz frequency where Debye-type dipolar relaxation of molecules arises.[53] Figure 14a shows the variation in the parallel and perpendicular components of dielectric permittivity with respect to temperature for pure and composite systems, where $\varepsilon_{\parallel}$ was evaluated at 40 V with $\varepsilon_{\perp}$ at 0 V DC bias. $\varepsilon_{\parallel}$ increased slightly in the case of VTO-MSE-dispersed 8CB as compared with pure 8CB, while there were no significant changes in $\varepsilon_{\perp}$. The plot of $\Delta\varepsilon$ with temperature for the pure and composite samples is shown in Fig. 14b. The value of $\Delta\varepsilon$ decreases with increasing temperature because of the disordering of LC molecules. In addition, the value increases in the nanocomposite mixed samples relative to the pure sample. The $\Delta\varepsilon$ is proportional to the order parameter, according to the Maier and Meier theory.[54,55] On dispersion of the VTO-MSE nanocomposite in 8CB, the order parameter increases, and hence $\Delta\varepsilon$ increases. Also, it was observed that the transition temperature of VTO-MSE-mixed 8CB was slightly increased by 1°C for 0.5 wt.% and 1 wt.% due to the change in the order parameter of the molecules.

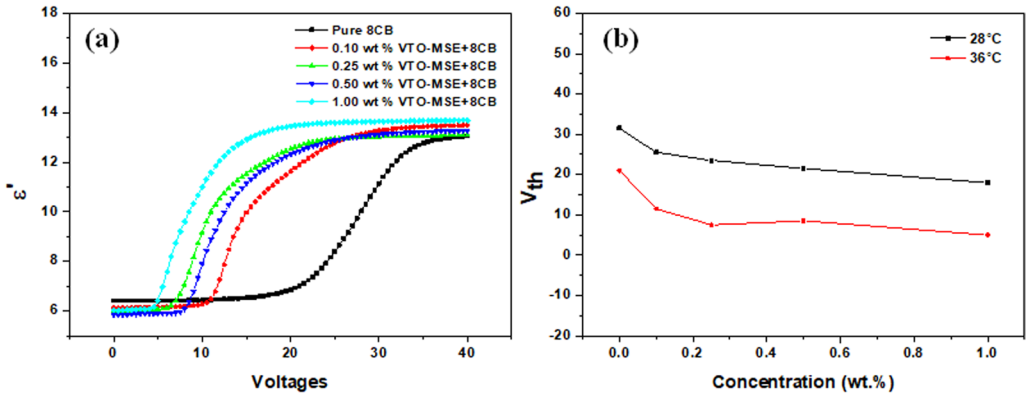

Fig. 15 Variation in (a) dielectric permittivity (ε') with respect to voltage for nematic phase and (b) threshold voltage with respect to concentration for smectic and nematic phases.

Threshold Voltage

The threshold voltage (V_{th}) is the voltage at which the LC molecules orient themselves in the direction of the electric field applied to the sample cell. Figure 15a shows the variation in ε' with respect to the voltage in the N phase for the pure and composite samples. V_{th} has been calculated using this graph and has been plotted at different concentrations of VTO-MSE nanocomposite for SmA (28°C) and N (36°C) as shown in Fig. 15b.

It was observed that the value of V_{th} decreased for the composite sample as compared with pure 8CB and remained almost constant with the increase in the concentration of the VTO-MSE nanocomposite due to the suppressed screening effect caused by the trapping of ions on the surface of the nanocomposite.[51] Further, V_{th} is inversely proportional to the $\Delta\varepsilon$, and because $\Delta\varepsilon$ increases with the dispersion of VTO-MSE in 8CB, V_{th} decreases.[53] This indicates that the switching time of the LC molecules decreases and they respond more rapidly to the applied voltage.

Conclusion

In this work, we have synthesized a VTO-MSE nanocomposite using a hydrothermal process and dispersed it in an 8CB LC material. Different concentrations of the VTO-MSE–8CB composite (0.1 wt.%, 0.25 wt.%, 0.5 wt.% and 1 wt.%) were prepared and their optical textures were observed using a cross-polarized optical microscope. The uniform micrographs obtained from this study suggest the homogeneous alignment of molecules on the dispersion of nanocomposites in the host LC material. The frequency-dependent dielectric parameters (ε', ε'' and tan δ) were evaluated using dielectric spectroscopy in the range of 20 Hz–2 MHz. The values of ε' and ε'' were found to be reduced in the case of the VTO-MSE nanocomposite mixed with 8CB in the low-frequency region due to the space charge polarization and ion trapping effect. The relaxation frequencies shift towards the low-frequency side in the composite system due to the decrease in the mobile ion density. Dielectric anisotropy was also calculated and found to increase in the nanocomposite dispersed system, which is attributed to the increased ordering of LC molecules. The threshold voltage was found to decrease in the VTO-MSE-dispersed 8CB samples, indicating the fast switching of molecules upon the addition of the nanocomposite. These findings may be beneficial for the fabrication of display devices with reduced ionic impurities and fast responses.

Conflict of interest The authors declare that they have no conflict of interest.

References

1. H.K. Bisoyi and Q. Li, Liquid crystals: versatile self-organized smart soft materials. *Chem. Rev.* 122, 4887 (2022).
2. T. Kato, N. Mizoshita, and K. Kishimoto, Functional liquid crystalline assemblies: self-organized soft materials. *Angew. Chem. Int. Ed.* 45, 38 (2006).
3. J.W. Goodby, I.M. Saez, S.J. Cowling, V. Gortz, M. Draper, A.W. Hall, S. Sia, G. Cosquer, S.E. Lee, and E.P. Raynes, Transmission and amplification of information and properties in nanostructured liquid crystals. *Angew. Chem. Int. Ed.* 47, 2754 (2008).
4. M.J. Stephen and J.P. Straley, Physics of liquid crystals. *Rev. Mod. Phys.* 46, 617 (1974).
5. S. Singh, *Liquid crystals fundamentals* (Singapore: World Scientific, 2002).
6. D. Andienko, Introduction to liquid crystals. *J. Mol. Liq.* 267, 520 (2018).
7. S.P. Yadav, R. Manohar, and S. Singh, Effect of TiO_2 nanoparticles dispersion on ionic behaviour in nematic liquid crystal. *Liq. Cryst.* 42, 1095 (2015).
8. V. Reiffenrath, U. Finkenzeller, E. Poetsch, B. A. Rieger, D. Coates, in *SPIE Proceedings* (1990), p. 84

9. M. Urbanski, On the impact of nanoparticle doping on the electro-optic response of nematic hosts. *Liq. Cryst. Today* 24, 102 (2015).
10. M. Urbanski and J.P.F. Lagerwall, Nanoparticles dispersed in liquid crystals: impact on conductivity, low-frequency relaxation and electro-optical performance. *J. Mater. Chem. C* 4, 3485 (2016).
11. J. Prakash, S. Khan, S. Chauhan, and A.M. Biradar, Metal oxide-nanoparticles and liquid crystal composites: A review of recent progress. *J. Mol. Liq.* 297, 112052 (2020).
12. L. Lisetski, M. Soskin, N. Lebovka, in *Springer Proceedings in Physics* (2015), p. 243.
13. A. Kumar, D.P. Singh, and G. Singh, Recent progress and future perspectives on carbon-nanomaterial-dispersed liquid crystal composites. *J. Phys. D Appl. Phys.* 55, 083002 (2022).
14. G. Yadav, R. Katiyar, G. Pathak, and R. Manohar, Effect of ion trapping behavior of TiO_2 nanoparticles on different parameters of weakly polar nematic liquid crystal. *J. Theor. Appl. Phys.* 12, 191 (2018).
15. Y.S. Ha, H.J. Kim, H.G. Park, and D.S. Seo, Enhancement of electro-optical properties in liquid crystal devices via titanium nanoparticle doping. *Opt. Express* 20, 6448 (2012).
16. D.P. Shcherbinin and E.A. Konshina, Impact of titanium dioxide nanoparticles on purification and contamination of nematic liquid crystals. *Beilstein J. Nanotechnol.* 8, 2766 (2017).
17. B. Liua, X. Wang, G. Cai, L. Wen, Y. Song, and X. Zhao, Low temperature fabrication of V-doped TiO_2 nanoparticles, structure and photocatalytic studies. *J. Hazard. Mater.* 169, 1112 (2009).
18. N. Khatun, R. Anita, and S. Sen. Amin, Bandgap tuning by lattice distortion in V and Ga doped TiO_2. *Integr. Ferroelectr.* 194, 91 (2018).
19. E.D. Hanson, L.M. Lilley, J.D. Cain, S. Hao, E. Palacios, K. Aydin, C. Wolverton, T. Meade, and V.P. Dravid, Phase engineering and optical properties of 2D MoSe2: promise and pitfalls. *Mater. Chem. Phys.* 225, 219 (2019).
20. R. Sivasamy, F. Quero, K.P. Gil, K.M. Batoo, M. Hadi, and E.H. Raslam, Comparison of the electronic, optical and photocatalytic properties of MoSe2, InN, and MoSe2/InN heterostructure nanosheet-A first-principle study. *Mater. Sci. Semicond. Process.* 131, 105861 (2021).
21. H. Yoo, K. Heo, M.H.R. Ansari, and S. Cho, Recent advances in electrical doping of 2D semiconductor materials: methods, analyses, and applications. *Nanomaterials* 11, 832 (2021).
22. O. Melo, Y. Gonzalez, A.C. Font, P. Galan, A. Ruediger, M. Sanchez, C.C. Mola, G. Santana, and V.T. Costa, Optical and electrical properties of MoO_2 and MoO_3 thin films prepared from the chemically driven isothermal close space vapor transport technique. *J. Phys. Condens. Matter* 31, 295703 (2019).
23. A.V. Avani and E.I. Anila, Recent advances of MoO_3 based materials in energy catalysis: applications in hydrogen evolution and oxygen evolution reactions. *Int. J. Hydrogen Energy* 47, 20475 (2022).
24. H. Zhou, Y. Shao, Z. Zhou, Y. Yang, J. He, L. Jiang, D. Chen, Y. Chen, Z. Yan, and J. Wang, Bio-inspired V-TiO_2 architectures with regulable surface ultrastructure for visible-light photocatalytic selective oxidation of cyclohexane. *Appl. Surf. Sci.* 622, 56957 (2023).
25. N. Wazir, R. Liu, C. Ding, X. Wang, X. Ye, X. Lingling, T. Lu, L. Wei, and B. Zou, Vertically stacked $MoSe_2$/MoO_2 nanolayered photodetectors with tunable photoresponses. *ACS Appl. Nano Mater.* 3, 7543 (2020).
26. K. Pal, A. Si, G.S.E. Sayyad, M.A. Elkodous, R. Kumar, A.I.E. Batal, S. Kralj, and S. Thomas, Cutting edge development on graphene derivatives modified by liquid crystal and CdS/TiO_2 hybrid matrix: optoelectronics and biotechnological aspects. *Crit. Rev. Solid State Mater. Sci.* 46, 385 (2020).
27. S.L. Guo, S.N. Lai, and J.M. Wu, Strain-induced ferroelectric heterostructure catalysts of hydrogen production through piezophototronic and piezoelectrocatalytic system. *ACS Nano* 15, 16106 (2021).
28. R. Guegan, D. Morineau, R. Lefort, W. Beziel, M. Guendouz, L. Noirez, A. Henschel, and P. Huber, Rich polymorphism of a rod-like liquid crystal (8CB) confined in two types of unidirectional nanopores. *Eur. Phys. J. E* 26, 261 (2008).
29. M. Gholamveysi, M. Ghodrati, M. Mousavi, A.P. Khomami, J.B. Ghasemi, M.M. Habibi, M.S. Gohari, P. Norouzi, and X. Li, $MoSe_2$ nanoflakes decorated ZnO nanorods: an effective photoelectrode with S-scheme heterojunction for photoelectrocatalytic degradation of tetracycline and rhodamine B. *Surf. Interfaces* 40, 103146 (2023).
30. H. Mittal, A. Kumar, and M. Khanuja, In-situ oxidative polymerization of aniline on hydrothermally synthesized $MoSe_2$ for enhanced photocatalytic degradation of organic dyes. *J. Saudi Chem. Soc.* 23, 836 (2019).
31. A. Chithambararaj and A.C. Bose, Hydrothermal synthesis of hexagonal and orthorhombic MoO_3 nanoparticles. *J. Alloys Compd.* 509, 8105 (2011).
32. B. Gowtham, V. Ponnuswamy, G. Pradeesh, J. Chandrasekaran, and D. Aradhana, MoO_3 overview: hexagonal plate-like MoO_3 nanoparticles prepared by precipitation method. *J. Mater. Sci.: Mater. Electron.* 29, 6835 (2018).
33. Y. Sun, Z. Zhang, L. Liu, and X. Wang, FTIR, Raman and NMR investigation of CaO-SiO_2-P_2O_5 and CaO-SiO_2-TiO_2-P_2O_5 glasses. *J. Non-Cryst. Solids* 420, 26 (2015).
34. A. Chithambararaj and A.C. Bose, Investigation on structural, thermal, optical and sensing properties of meta-stable hexagonal MoO_3 nanocrystals of one dimensional structure. *Beilstein J. Nanotechnol.* 2, 585 (2011).
35. Y. Xia, W. Cui, R. Ji, C. Huang, Y. Huang, H. Zhang, F. Xu, P. Huang, B. Li, and L. Sun, Design and synthesis of novel microencapsulated phase change materials with enhancement of thermal conductivity and thermal stability: Self-assembled boron nitride into shell materials. *Colloids Surf A Physicochem Eng Asp* 586, 124225 (2020).
36. X. Ruan, Y. Yang, W. Liu, X. Ma, C. Zhang, Q. Meng, Z. Wang, F. Cui, J. Feng, F. Cai, Y. Yuan, and G. Zhu, Mechanical bond approach to introducing self-adaptive active sites in covalent organic framework for zinc-catalyzed organophosphorus degradation. *ACS Cent. Sci.* 7, 1698 (2021).
37. A. Gridyakina, N. Kasian, M.S. Chychłowski, M. Kajkowska, and P. Lesiak, Advances in multicomponent systems: liquid crystal/nanoparticles/polymer. *Mater. Today Phys.* 38, 101258 (2023).
38. A.K. Jain and R.R. Deshmukh, Effects of dye doping on electro-optical, thermo-electro-optical and dielectric properties of polymer dispersed liquid crystal films. *J. Phys. Chem. Solids* 160, 110363 (2022).
39. P. Priscilla, P. Malik, S.A. Kumar, R. Castagna, and G. Singh, Recent advances and future perspectives on nanoparticles-controlled alignment of liquid crystals for displays and other photonic devices. *Crit. Rev. Solid State Mater. Sci.* 48, 57 (2013).
40. J. Prakash, A. Kumar, and S. Chauhan, Aligning liquid crystal materials through nanoparticles: a review of recent progress. *Liquids* 2, 50 (2022).
41. H. Zhang, Z. Miao, and W. Shen, Development of polymer-dispersed liquid crystals: From mode innovation to applications. *Compos. - A: Appl. Sci. Manuf.* 163, 107234 (2022).
42. C.J. Hsu, B.P. Singh, P. Selvaraj, M. Antony, R. Manohar, and C.Y. Huang, Superior improvement in dynamic response of liquid crystal lens using organic and inorganic nanocomposite. *Sci. Rep.* 11, 1 (2021).
43. L. Chauhan, A.K. Shukla, and K. Sreenivas, Dielectric and magnetic properties of Nickel ferrite ceramics using crystalline powders derived from DL alanine fuel in sol-gel auto-combustion. *Ceram. Int.* 41, 8341 (2015).

44. Y.L. Nian, P.C. Wu, and W. Lee, Optimized frequency regime for the electrohydrodynamic induction of a uniformly lying helix structure. *Photonics Res.* 4, 227 (2016).
45. A. Rani, S. Chakraborty, and A. Sinha, Effect of CdSe/ZnS quantum dots doping on the ion transport behavior in nematic liquid crystal. *J. Mol. Liq.* 342, 117327 (2021).
46. G. Jamwal, J. Prakash, A. Chandran, J. Gangwar, A. K. Srivastava and A. M. Biradar, in *AIP conference proceedings* (2015), p. 030065
47. S. Uemura, Ionic contribution to the complex dielectric constant of a polymer under dc bias. *J. Polym. Sci.* 10, 2155 (1972).
48. H.H. Liu and W. Lee, Time-varying ionic properties of a liquid-crystal cell. *Appl. Phys. Lett.* 97, 023510 (2010).
49. C.G. Koops, On the dispersion of resistivity and dielectric constant of some semiconductors at audio frequencies. *Phys. Rev.* 83, 121 (1951).
50. A.A. Sattar and S.A. Rahman, Dielectric properties of rare earth substituted Cu-Zn ferrites. *Phys. Status Solidi (a)* 200, 415 (2003).
51. G. Kocakulah, G. Onsal, K. Gokşen, I. Ercan, and O. Koysal, Concentration effect of cadmium selenide sulphide/zinc sulphide quantum dots on electro-optic and dielectric properties in nematic liquid crystals composite. *Phys. B: Condens. Matter.* 550, 47 (2018).
52. Y. Lin, A. Daoudi, F. Dubois, A.S. Mera, C. Legrand, and R. Douali, Correlation between dielectric properties and phase transitions of 8CB/$Sn_2P_2S_6$ liquid crystal nanocolloids. *J. Mol. Liq.* 232, 123 (2017).
53. K.K. Vardanyan, A. Daykin, and B. Kilmer, Study on cyanobiphenyl nematic doped by silver nanoparticles. *Liq. Cryst.* 44, 1240 (2017).
54. W. Maier and G. Meier, A simple theory of the dielectric are some homogeneous criteria oriented liquid crystal phases of nematic type. *Z. Naturforsch. A* 16, 262 (1961).
55. H. Kresse, *Advances in liquid crystals* (New York: Academic Press, 1983).